



# Capacity Difference of Circular Hollow Section X-joints Under Brace Axial Compression and Tension

Bida Zhao<sup>1,2</sup> · Chengqing Liu<sup>2,3</sup> · Zeyang Yao<sup>1</sup> · Yangzheng Cai<sup>1</sup>

Received: 22 October 2019 / Accepted: 5 July 2020 / Published online: 10 July 2020  
© Korean Society of Steel Construction 2020

## Abstract

In the current regulations, there are two methods to describe the relationship between the two capacities of circular hollow section (CHS) X-joints under brace compression ( $N_{uc}$ ) and brace tension ( $N_{ut}$ ):  $N_{ut} = N_{uc}$  and  $N_{ut} = fN_{uc}$  ( $f$  is a coefficient larger than 1.0). In order to study the difference between  $N_{uc}$  and  $N_{ut}$  of the X-joints, two experimental tests (monotonic compression load and cyclic axial load) and finite element (FE) analysis are performed to study the difference between  $N_{uc}$  and  $N_{ut}$ . Test results show that the ultimate capacity is close to the resistance load corresponding to the connection deformation of 3% of chord diameter (limit deformation criterion). Both two specimens showed good deformability and ductility. The final failure modes are chord wall buckling and chord wall tearing for the specimens under monotonic compression load and cyclic axial load, respectively. Test and FE results indicate that  $N_{ut}$  is significantly larger than the corresponding  $N_{uc}$ , and the ratio  $N_{ut}/N_{uc}$  increases as the chord radius-to-thickness ratio  $\gamma$  increases. It is also found that the ratio  $N_{ut}/N_{uc}$  increases as the brace-to-chord diameter ratio  $\beta$  increases, especially  $\beta$  larger than 0.8. Based on test and FE data, a new equation for the ratio  $N_{ut}/N_{uc}$  is proposed to overcome the defect of the current specifications that cannot consider the influence of  $\beta$ . The equation is proved to be reasonable by tests and FE results.

**Keywords** Circular hollow section (CHS) X-joints · Brace compression · Brace tension · Tensile-to-compressive capacity ratio · Experimental test · Finite element (FE) analysis

## 1 Introduction

Unstiffened tubular joint are used extensively in all kinds of offshore and civil engineering structures, but the ultimate strength of these unstiffened tubular joints are usually relative low due to their structural characteristics of the brace welded

directly to the chord surface. Hence, strength and suitable strengthening techniques are one of the research priorities of tubular joints (Liu et al. 2017, 2018; Liu and Ma 2017). Based on pressure vessel plastic limit analysis concept (Gerdeen 1980), Choo et al. (2003) presents a new method to define the capacity of thick-walled circular hollow section (CHS) unstiffened X-joint under brace axial force. It is found that the capacity is correlate to the results obtained by the deformation limit criterion suggested by Lu et al. (1994). Zhao et al. (2020) investigated the ultimate capacity of an eccentric rectangular hollow section (RHS) X-joint under out-of-plane bending, and proposed a prediction equation for the flexural capacity. Although the equation agrees well with the test and FE results, but only one physical X-joint specimen and requires more test data for further verification. Liu et al. (2020), Liu and Fang (2020) carried out theoretical analysis and FE analysis to study the effect of brace-to-chord out-of-plane angle (BCOPA) on the capacity of multi-planar CHS X-joints under out-of-plane bending moment (OPBM). Furthermore, the capacity equation of current specification only applicable to uniplanar CHS X-joints was improved and extended to

✉ Chengqing Liu  
lcqjd@swjtu.edu.cn

Bida Zhao  
zhaobida@126.com

Zeyang Yao  
zjgydxyzy@163.com

Yangzheng Cai  
469909934@qq.com

<sup>1</sup> College of Civil Engineering and Architecture, Zhejiang University of Technology, Hangzhou 310014, China

<sup>2</sup> School of Civil Engineering, Southwest Jiaotong University, Chengdu 610031, China

<sup>3</sup> Key Laboratory of High-Speed Railway Engineering of Ministry of Education, Chengdu 610031, China

the multi-planar X-joints by introduced a spatial effect factor, and the improved specification was verified by FE results. Feng and Young (2015) carried out study on capacity of cold-formed stainless steel RHS and square hollow section (SHS) T- and X-joints under brace compression, and proposed design formulae for these stainless steel tubular joints by modifying the existing formulae of carbon steel tubular joints. Forti Nádia et al. (2015) carried out study on the capacity of multi-planar CHS KK-joints under symmetrically loaded, and proposed the capacity formulae. Zhao et al. (2019a, b) carried out study on the out-of-plane bending behavior of CHS X-joints. In addition to the static behavior of the unstiffened tubular joints, the strengthening technique on tubular joints also received attention. Iskander et al. (2017) were studied the capacity of CHS T-joints strengthened by through-bolts, and found that using only one through bolt can increase the capacity of unstiffened T-joint by 35%. Chen et al. (2016) investigated the performance of double-skin CHS X-joints subjected to brace compression, and proposed capacity prediction equations for these joints. Nassiraei et al. (2016) analyzed the main factors (e.g., the size of doubler plate) affecting the static behavior of doubler plate strengthened CHS T/Y-joints under brace axial force. The results showed that the capacity and stiffness of the joints were significantly enhanced by the doubler plate, and the plate can also improve failure modes of the joints. Lan et al. (2016) investigated ultimate capacity of CHS DT-joints (strengthen by internally ring-stiffened) under brace axial force. Lesani et al. (2014) studied on the behavior of the CHS T-joints strengthened with fiber reinforced polymer (FRP), and found that the FRP installation can significantly improve the ultimate capacity of the T-joints. Lesani et al. (2015) also studied on the rehabilitation of CHS T- and Y-joints wrapped with FRP. Xie et al. (2019) performed theoretical and FE studied on the ultimate strength of concrete-filled steel tube (CFST) K-joints, and the results showed that the strength of the joints can be obviously improved by using core concrete. Liu et al. (2019) proposed a four-spring assemblage model to express the moment-rotation behavior of diagrid non-stiffened concrete filled steel tubular (CFST) joints. However, there are some defects in the four-spring model including too many artificial assumptions and too many parameters (sixteen). In addition, only FE results were used to verify the rationality of the four-spring model, lack of experimental verification. Hosseini and Rahnavard (2020) performed 18 FE model analysis to investigate the behavior of the innovative collar rigid H-beam/box-column connections. The results showed that the proposed connections with long collar area exhibit significantly better seismic performance than the corresponding connections with short collar, such as main plastic deformation and stress concentration of the former occurs in the beam not the connection area. Rahnavard et al. (2015) carried out numerical study on seismic behavior of welded beam-column connections with different reduced beam flange (RBF) methods. The results

showed that RBS with varied holes has more ductile and dissipate energy capacity than other types of RBS connections, and also has minimum of out-of-plane buckling. Hassanipour et al. (2016) performed numerical investigate on the seismic behavior of welded beam-column connections with reduced beam web (RBW), and found that the connections with RBW have more ductile and dissipate energy.

Unstiffened CHS X-joints, two braces usually with the same section size and subjected the same value of forces, is one of most common form of joints in tubular structures. In most current specifications, the capacity prediction formulae of CHS X-joint under brace axial compression ( $N_{uc}$ ) based on the ring model, originally developed by Togo (1967). However, there are significantly different with regard to the capacity formulae of the X-joint under brace tension ( $N_{ut}$ ) mentioned in the current specifications. One, such as the specification of EC3 (2005), considered that the joint capacity under brace tension is the same as that under brace compression, i.e.,  $N_{ut} = N_{uc}$ . The other, such as the specification of Chinese standard GB 50017-2017 (2018), believed that  $N_{ut} > N_{uc}$  and the equation of  $N_{ut}$  is expressed as  $fN_{uc}$ . Here  $f$  is a coefficient greater than 1.0 and varies with the chord radius-to-thickness ratio  $\gamma$ . However, it is necessary to further study on the difference between the compressive capacity and the tensile capacity of the X-joints, e.g., whether the difference is small, and the difference is only related to the geometric parameter  $\gamma$ .

The paper aims to study the behavior difference of CHS X-joints subjected to brace compression and brace tension. Two CHS X-joints experimental test, brace axial quasi-static cyclic loaded and brace axial static compression loaded, are first performed to investigate the performance of the X-joint under the brace axial tension and compression loaded. The experimental test is also utilized to verify the numerical simulation method. Then, the influence of brace loaded condition (tension and compression) on the ultimate capacity of the X-joint is investigated by FE parametric analysis results of tensile-to-compressive capacity ratio  $N_{ut}/N_{uc}$ . Experimental and FE results show that the ratio  $N_{ut}/N_{uc}$  is significantly greater than 1.0. The ratio  $N_{ut}/N_{uc}$  not only related to the parameter  $\gamma$  but also to another important geometric parameter  $\beta$  (the ratio of brace diameter to chord diameter) especially when  $\beta \geq 0.8$ . Furthermore, A new equation (considering the influence of  $\gamma$  and  $\beta$ ) is proposed to more accurately predict the ratio  $N_{xut}/N_{xuc}$  of the X-joints with large  $\beta$  ( $\geq 0.8$ ).

## 2 Experimental Test

### 2.1 Specimen's Geometry and Material Properties

Figure 1 shows the detail of two specimens and the test displacement transducers arrangement (from D1 to D6). The

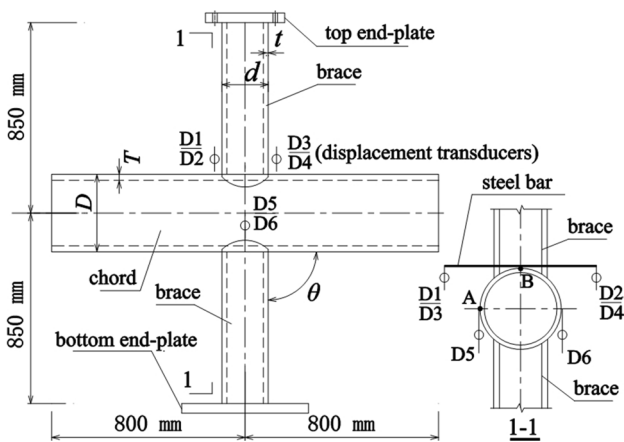


Fig. 1 Specimen and displacement transducers location

geometric characteristics of the specimens are as follow: the chord length is  $l_c = 1600$  mm, the length between the two brace end is  $l_b = 1700$  mm. Other geometric parameters are listed in Table 1, which including the ratio of brace diameter to chord diameter  $\beta = d/D$ , chord radius-to-thickness ratio  $\gamma = 0.5D/T$ , brace-to-chord wall thickness ratio  $\tau = t/T$ , the angle between brace and chord  $\theta$ . It is noted that the suffixes MC and AR in the Table 1 indicate the two specimens under monotonic axial compression loading and cyclic axial loading respectively. As for the material properties, i.e., yield strength ( $f_y$ ), ultimate strength ( $f_u$ ), elastic modulus ( $E$ ), and fracture elongation ( $\zeta$ ), obtained from tension coupon tests are listed in Table 2.

### 2.2 Test Setup

Figure 2 shows the arrangement of the X-joints under brace axial loaded. Brace ends are welded end-plates, and each specimen is stand up with the chord horizontally. The bottom end-plate of brace is fixed to the bottom strong reaction beam through four anchor bolts, and the top end-plate of brace is connected to servo hydraulic actuator by four high-strength bolts. One advantage of the above loading device is that the load at two brace ends can be applied synchronously using only one hydraulic actuator movement.

Static monotonous compression load is employed for the test program of the specimen CHS-MC. Quasi-static cyclic load (displacement control) is employed for the test program of the specimen CHS-AR. For the beginning three

Table 2 Average measured material properties

Section (mm)	$f_y$ (MPa)	$f_u$ (MPa)	$E$ (GPa)	$\zeta$ (%)
244.6×7.96 CHS	375.3	545.1	209	32.7
202.8×6.80 CHS	372.1	550.3	213	31.3
146.1×6.22 CHS	373.4	558.4	216	30.8

cycles, CHS-AR is tested with displacement amplitudes of  $\pm 2.5$  mm,  $\pm 5$  mm and  $\pm 7$  mm, here 5 mm is the displacement corresponding to the yield load  $N_{yFE}$  obtained from numerical simulation result before the test. Then the displacement amplitude of each cyclic loading increased by 3 mm from the previous level (one cycle per level) until the X-joint failed, e.g., the amplitudes of the fourth and the fifth cycles are  $\pm 10$  mm and  $\pm 13$  mm respectively.

### 2.3 Experimental Phenomena and Failure Modes

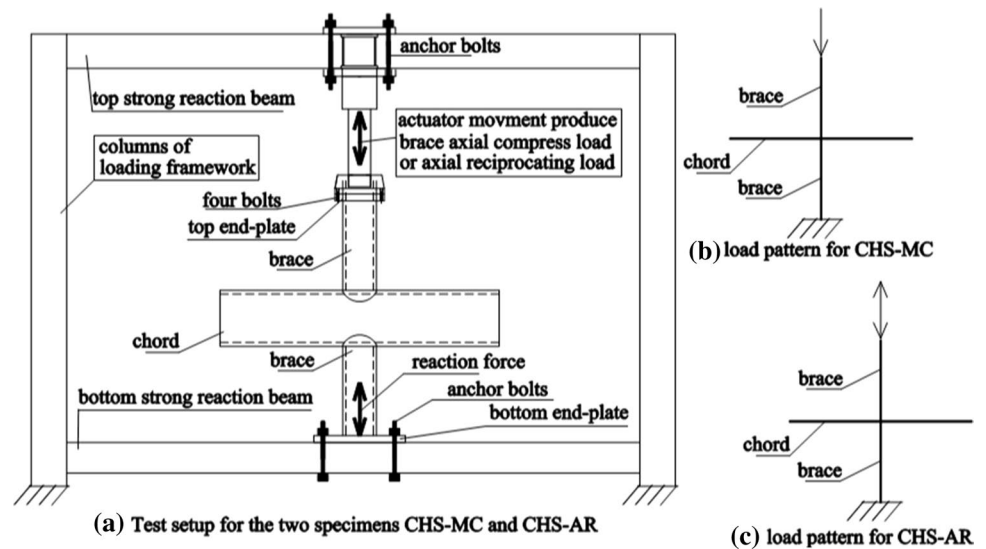
For the specimen CHS-MC (static monotonous compression loaded), recognizable concave deformation is observed on the saddle region of the chord when the load is about 385 kN. Subsequently, the concave has been increasing, and the load is first increases to the peak of 425.5 kN then gradually decreases. The finally failure mode of CHS-MC is buckling of the chord wall near brace/chord intersection, as shown in Fig. 3a.

In the CHS-AR test (brace axial cyclic loaded), yielding is first observed at the chord wall near the saddle during the second loading cycle (the yield load  $N_y$  is 160 kN). When the loading displacement reached  $\pm 13$  mm, the peak value of tension load is larger than that of compression load. Subsequently, the difference between the two peaks of each loading cycle is gradually increased until the specimen reach the ultimate capacity (during the  $\pm 22$  mm loading cycle). At the same loading level, a tiny crack is first observed at the chord wall near the saddle region which affected by welding residual stress. After that, the resistance gradually decreased with crack extension. When the  $\pm 37$  mm loading cycle is reached, the resistance decreased to approximately 70% of the peak force due to the cracks propagation. The specimen finally failed due to the tearing of the chord wall near the brace/chord intersection, as shown in Fig. 3(b).

Table 1 Average measured geometric properties

Specimen	$D$ (mm)	$d$ (mm)	$T$ (mm)	$t$ (mm)	$\beta$	$\gamma$	$\tau$	$\theta$ (°)
CHS-MC	244.6	202.8	7.96	6.80	0.83	15.3	0.85	90
CHS-AR	244.6	146.1	7.96	6.22	0.60	15.3	0.78	90

**Fig. 2** Test setup and load pattern



## 2.4 Axial Force-Connection Deformation Curves

The axial force-connection deformation ( $N$ - $\delta$ ) curves of two specimens CHS-MC (static monotonous loading) and CHS-AR (quasi-static cyclic loading) are presented in Fig. 4. The abscissa is connection deformation  $\delta$ , which can be obtained by two methods. According to Voth and Packer (2012),  $\delta$  is defined as the vertical distance change between the crown point (point B in Fig. 1) and the center point of the chord (point A in Fig. 1), i.e.,  $\delta = \delta_B - \delta_A = (\delta_1 + \delta_2 + \delta_3 + \delta_4)/4 - (\delta_5 + \delta_6)/2$ . Here  $\delta_1$  to  $\delta_6$  are the displacement measured by the six transducers (D1-D6 in Fig. 1). The above method also named as direct method. In contrast, indirect method (another method) considers  $\delta = (\delta_{tlp} - \delta_{ub} - \delta_{bb})/2$ ,  $\delta_{tlp}$  is the displacement at the loading end obtained by the actuator's own displacement transducer,  $\delta_{ub}$  and  $\delta_{bb}$  are the axial deformations of two braces calculated by the elastic

bar theory. The ordinate in Fig. 4 is brace axial force, and positive and negative values indicate tension and compression respectively.

It can be inferred from Fig. 4a that the  $N$ - $\delta$  curves obtained by the two methods are very close to each other while  $\delta < 11$  mm. It should be noted that the  $\delta$  obtained by direct method is less than 15 mm. The reason is that the six transducers (D1 to D6) are deviated the original position due to the excessive deformation of chord wall in the post-loading, resulting in wrong displacements for the  $\delta_1$ - $\delta_6$ , which should be deleted.

Similarly, Fig. 4b shows that the hysteretic curves obtained by direct method correlates reasonably well with the results of indirect method. Moreover, the hysteretic curves are exhibited stability and no pinching effect before the cracks occurred. The ultimate capacity ( $N_u$ ) is obviously less than the force corresponding to the nominal yield strength of the

**Fig. 3** Failure modes of test specimens

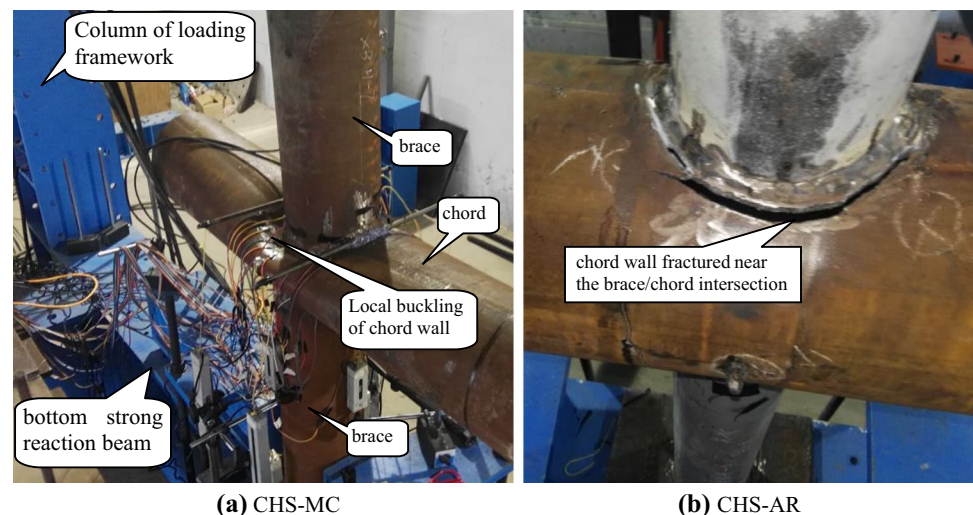
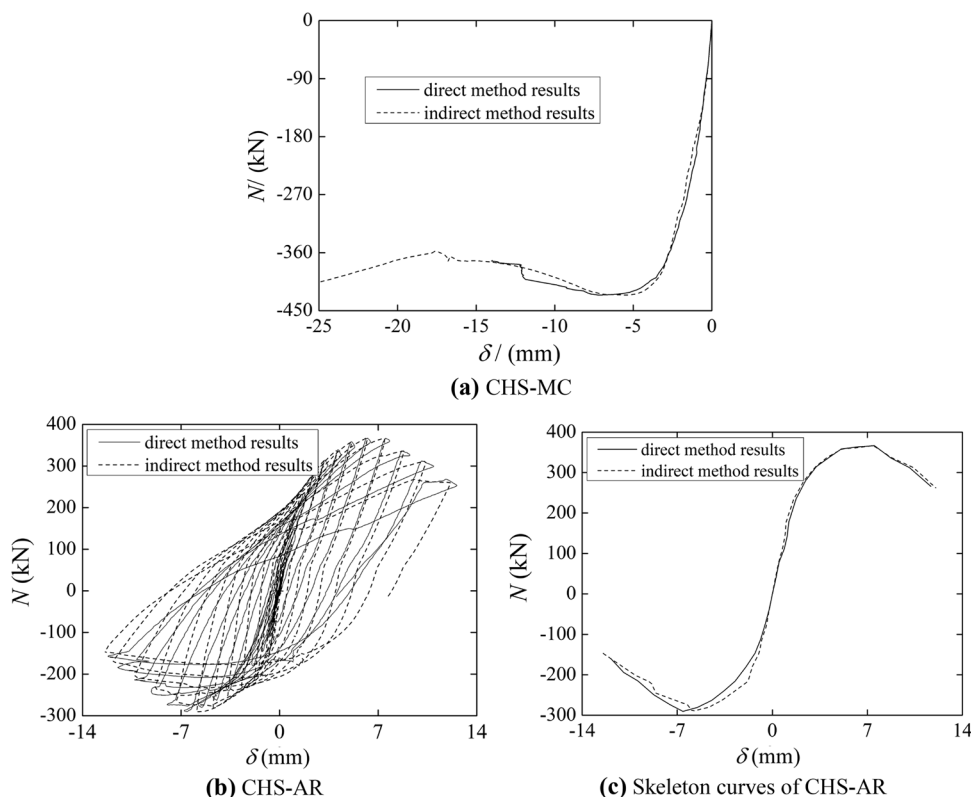


**Fig. 4** Brace axial force verse connection deformation relationships ( $N-\delta$  curves) of the two specimens



brace ( $N_{by} = 984.3$  kN), which means the braces mostly stayed elastic. Therefore, energy dissipation, plastic development and ductility demand of the specimen CHS-AR are mainly provided by the chord wall near at brace/chord intersection.

**2.5 Ultimate Strength and Ductility**

Ultimate capacity from test are listed in Table 3, where  $N_{ut}$  and  $N_{uc}$  are tension strength and compression strength respectively. The test results are also compared with the corresponding capacity predicted by EC3 (2005), GB 50017-2017 (2018) and AIJ (1997) expressed by Eqs. (1), (2) and (3) respectively. It is noted that these three equations are based on the chord wall plastification failure mode of CHS X-joints. In the three equations and Table 3, subscripts EC3, GB and AIJ indicate specifications of EC3, GB50017-2017 and AIJ respectively; subscripts t and c indicate tension and compression respectively. For example,  $N_{EC3,c}$  is the compression capacity of CHS X-joints predicted by EC3. Moreover, the meanings

of other parameters (i.e.,  $\beta$ ) in the three equations are the same as the corresponding parameters in the Tables 1 and 2.

$$N_{EC3,t} = N_{EC3,c} = \frac{5.2f_y T^2}{(1 - 0.81\beta) \sin \theta} \tag{1}$$

$$\begin{cases} N_{GB,c} = \frac{5.45f_y T^2}{(1 - 0.81\beta) \sin \theta} \\ N_{GB,t} = 0.78(2\gamma)^{0.2} N_{GB,c} \end{cases} \tag{2}$$

$$\begin{cases} N_{AIJ,c} = \frac{8.24\gamma^{-0.1} f_y T^2}{(1 - 0.81\beta) \sin \theta} \\ N_{AIJ,t} = 0.71 \gamma^{0.3} N_{AIJ,c} \end{cases} \tag{3}$$

It can be seen from Table 3 that these design equations can well predict the ultimate compressive resistance for

**Table 3** Comparison between test capacities and predicted values (kN)

Specimens	$N_{uc}$	$N_{ut}$	$N_{EC3,c}$	$N_{EC3,t}$	$N_{GB,c}$	$N_{GB,t}$	$N_{AIJ,c}$	$N_{AIJ,t}$	$\frac{N_{EC3,c}}{N_{uc}}$	$\frac{N_{EC3,t}}{N_{ut}}$	$\frac{N_{GB,c}}{N_{uc}}$	$\frac{N_{GB,t}}{N_{ut}}$	$\frac{N_{AIJ,c}}{N_{uc}}$	$\frac{N_{AIJ,t}}{N_{ut}}$
CHS-MC	425.5	–	379.5	379.5	397.7	615.3	455.7	734.2	0.89	–	0.93	–	1.07	–
CHS-AR	290.3	366.6	240.4	240.4	251.8	389.6	289.7	466.7	0.83	0.65	0.87	1.06	1.00	1.27

the two specimens. As for the ultimate tensile resistance, the design equation of GB 50017-2017 gives a well prediction, the equation of AIJ gives a relative better but over-estimated prediction, the equation of EC3 gives a significantly underestimated prediction. It is implied that these strength equations, based on static monotonic loading, can also be applicable to cyclic loading (specimen CHS-AR). It also implies that the ultimate tensile capacity is obviously higher than ultimate compressive capacity. The difference between the tensile capacity and the compressive capacity are more detail in the Sect. 4.

Table 4 shows the ductility ratio, obtained from the  $N$ - $\delta$  curves (skeleton curves for CHS-AR) and defined as  $\mu = \delta_u / \delta_y$ , to evaluate the ductility supply of the X-joints under monotonous load and cyclic load. In the table,  $\delta_u$  is the connection deformation corresponding to the peak load  $N_u$ , and  $\delta_y$  is the yield connection deformation (Kurobane et al. 1984) corresponding to connection yield load  $N_y$  determined by the secant modulus  $0.779K_a$  ( $K_a$  is the initial stiffness of the X-joints under brace axial force). The subscripts + and – refer to the tension and compression respectively, and ‘direct’ and ‘indirect’ denote the results from direct method and indirect method respectively. It is observed that  $\delta_u$  is close to the 3% of chord diameter, which implied the ultimate capacity from test is close to the tubular joint capacity determined by the limit deformation proposed by Lu et al. (1994). It is also observed that the ductility ratios from direct method is close to that of indirect method results. The ductility ratios of CHS-AR shows that  $\mu$  is larger than  $\mu_+$ , which is mainly related to the obvious smaller compressive yield deformation  $\delta_{y-}$ .

### 3 Numerical Simulations

#### 3.1 Finite Element (FE) Model

The numerical study are conducted using FE program Abaqus (2016). According to the geometric sizes and configurations of the specimens, FE models are established (shown in Fig. 5). Both chord ends are free and one brace end is fixed to reflect the actual boundary conditions of the test, another brace end is applied static monotonic displacement

to simulate the brace axial force (compression or tension). With reference to some literature related to numerical simulation (e.g. Rahnavard et al. 2016, 2018; Naghavi et al. 2019) and combined with author’s numerical simulation comparison analysis, the element types and meshing of FE model are as follows. Eight-node reduced integration shell elements S8R (Abaqus 2016) are used in the FE models. A refined meshes (size is chord thickness  $T$ ) are used near the brace/chord intersection region to accurately capture the stress/strain distributions, and the other regions adopted rectangular mesh sizes with length and width are  $3T$  and  $T$  respectively.

During static analysis, geometric nonlinearity is considered by using the NIGEOM option (Abaqus 2016), and material nonlinearity is also considered through a classical plasticity model based on the Von Mises yield criterion and associated plastic flow. The stress–strain relationship of steel material is described by a bilinear kinematic hardening, which yield strength  $f_y$  and the elastic modulus  $E$  taken from the tensile coupon tests (Table 2), and the tangent modulus  $E_t$  equal to  $0.01E$  proposed by EC3 (2006). The welds is neglected in the FE analysis due to decreasing the actual thickness of the chord face which covered by the brace (i.e., conservative results for the capacity), and the distribution of residual stresses are difficult to estimated.

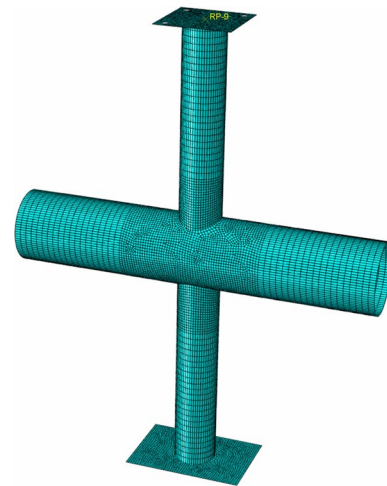


Fig. 5 Numerical simulation model with mesh layout

Table 4 Ductility ratio

Specimens	$\delta_{y+}$ (mm)	$\delta_{y-}$ (mm)	$\delta_{u+}$ (mm)	$\delta_{u-}$ (mm)	$\mu_+$	$\mu_-$
CHS-MC						
Direct	–	1.05	–	7.42	–	7.07
Indirect	–	0.84	–	5.81	–	6.92
CHS-AR						
Direct	2.37	1.43	7.53	6.58	3.18	4.60
Indirect	2.04	1.39	7.44	5.98	3.65	4.30

### 3.2 Comparison Against Experimental Results

Load-connection deformation ( $F-\delta$ ) curves of FE results are compared with the counterpart test results, as shown in Fig. 6. It is noted that the  $F-\delta$  curves of the specimen CHS-AR adopted skeleton curves to compare with the numerical simulations results from static monotonic brace axial loaded (including compression and tension). Moreover, the  $F$  and  $\delta$  from brace compression are also adopted positive values to facilitate comparison with the  $F-\delta$  curves of brace tension, and  $\delta$  are obtained by the indirect methods (Sect. 2.4). It can be seen from Fig. 6 that the FE results generally agree well with the test results, although there are some differences in the post-cracking behavior (strength deterioration) for the specimen CHS-AR. The main reason is that the fracture mechanism was not included in the FE modeling. Figure 6 also shows that the ultimate capacity from numerical simulation results is also very close to the corresponding test results. It is noted that the resistance corresponding to connection deformation ( $\delta$ ) of 3% of chord diameter is taken as the ultimate capacity if the  $F-\delta$  curves without pronounced peak loads. Generally, the above-mentioned FE analysis techniques are believed suitable for use as the following parametric analysis.

Furthermore, the tensile-to-compressive bearing capacity ratio ( $N_{ut}/N_{uc}$ ) of CHS-AR from test result and numerical simulation result are 1.27 and 1.39 respectively, which are relatively close to the values calculated by the specifications GB50017 and AIJ (1.55 and 1.61). However, the ratio  $N_{ut}/N_{uc}$  of CHS-MC from numerical simulation result is 2.34, which obviously larger than the calculated values of GB50017 and AIJ. Moreover, the ratio  $N_{ut}/N_{uc}$  of CHS-MC (2.34) is significantly larger than the corresponding ratio of CHS-AR (1.39). It is implied that the effect of  $\beta$  (the ratio of brace diameter to chord diameter) on the ratio ( $N_{ut}/N_{uc}$ ) cannot be neglected, because geometric parameter  $\beta$  is the most difference between CHS-MC and CHS-AR. However, the prediction equation for the ratio  $N_{ut}/N_{uc}$  in current specifications [Eqs. (2) and (3)] only considers the influence of

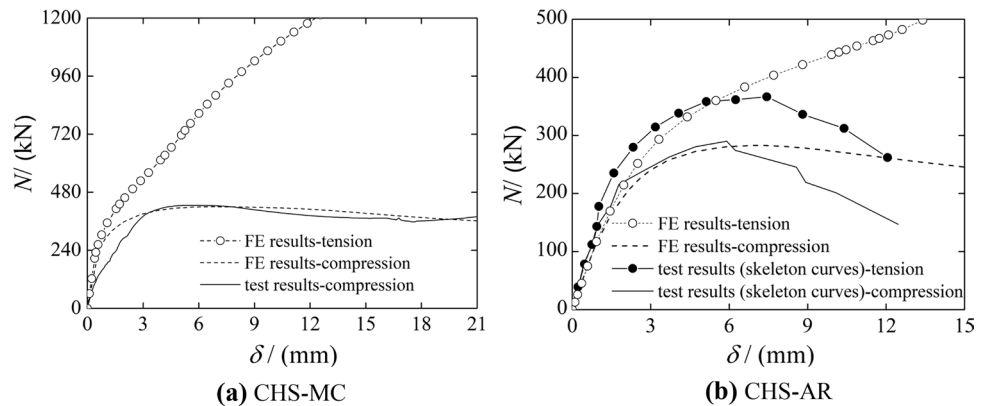
$\gamma$  (chord radius-to-thickness ratio), not considers the influence of  $\beta$ .

Figure 7 plots the contour of equivalent plastic strain ( $\epsilon_{eps}$ ) distribution on the joint-zone of the two specimens at the displacement level corresponding to test ultimate load or 0.03 time of chord diameter, the latter is only for specimen CHS-MC under brace tension due to no test results. Figure 7 shows that the X-joint with smaller  $\beta$  (specimen CHS-AR) develops high plastic strains (gray and red regions) concentrated in the saddle region, while the X-joint with larger  $\beta$  (specimen CHS-MC) develops more extensive plastic strains which distributed both in the saddle region and in the chord area between two saddles. This means that the performance of the X-joints with larger  $\beta$  are obviously different from those with smaller  $\beta$ . It can also be seen from Fig. 7 that the peak value of  $\epsilon_{eps}$  of the X-joint under brace tension is smaller than those under brace compression. Furthermore, compared with the X-joints under brace compression, the X-joints under brace tension develops more sufficient plasticity in the chord area between two saddles. It is indicated that the performance of the X-joints under brace tension is different from those X-joints under brace compression.

### 4 Analysis for the Tensile-to-Compressive Capacity Ratio

This section will study the difference between the tensile capacity (under brace tension) and compressive capacity (under brace compression) of CHS X-joints. The chord wall near the brace/chord intersection can taken as a 3D-shell structures. Brace compression will causes local buckling of the chord wall (the 3D-shell) led to decrease bearing capacity of the X-joints, which proved by the previous FE results (Fig. 7c) and test results (Fig. 3a). By contrast, the strain-hardening effect of mild steel and the membrane effect of chord wall (3D-shell) will help to improve the bearing capacity when the X-joints under brace tension, which proved by the test and FE results (Fig. 6). Furthermore, the

Fig. 6 Load-connection deformation ( $N-\delta$ ) curves comparison between test and FE results



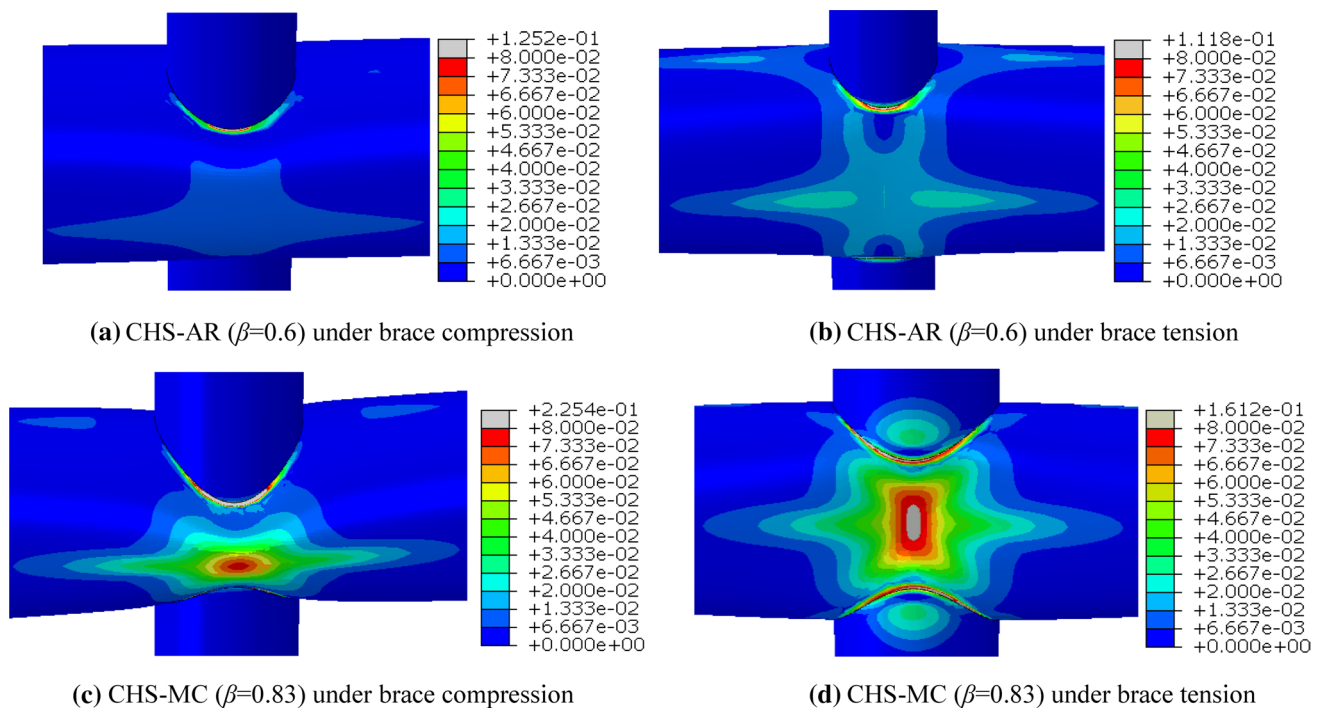


**Fig. 7** Comparison of equivalent plastic strain distributions of two specimen models under compression and tension

local buckling and the membrane effect will be more obvious as the thickness of chord wall decreased ( $\gamma$  increased). Therefore, the tensile-to-compressive capacity ratio  $N_{ut}/N_{uc}$  is increased as the parameter  $\gamma$  increased, which is reflected in the equations of the ratio  $N_{ut}/N_{uc}$  of the specifications GB50017 and AIJ [Eqs. (2) and (3)].

The performance of CHS X-joint is also greatly affected by the ratio  $\beta$ . The joint-zone of CHS X-joints with medium (or small)  $\beta$  can be simplified as a semicircular model under the load from brace axial force, as shown in Fig. 8b. However, as for the X-joints with large  $\beta$ , the brace axial forces are similar to applied directly to the two short arcs between the saddle points of the chord (arc  $A_1A_2$  and arc  $A_3A_4$  in Fig. 8b). Therefore, the behavior of the X-joints with large  $\beta$  is significantly different from that of the X-joints with medium (or small)  $\beta$ , which proved by the previous FE analysis results (Fig. 7) and leading difference in the ratio  $N_{ut}/N_{uc}$  of the two types CHS X-joints.

A parametric analysis with 40 FE models for CHS X-joints is carried out, in which  $D=245$  mm,  $\tau=0.8$ ,  $f_y=282$  Mpa,  $\theta=90^\circ$ ,  $\beta=0.3, 0.45, 0.6, 0.75, 0.8, 0.85, 0.9, 0.95$ ,  $\gamma=7, 10, 15, 25, 35$ . Then 40 data about the ratio  $N_{ut}/N_{uc}$  are obtained and utilized to investigate the effect of  $\gamma$  and  $\beta$  on the ratio  $N_{ut}/N_{uc}$ , as shown in Fig. 9. Figure 9a shows that a power function is able to reasonably fit  $N_{ut}/N_{uc}-\gamma$  curves, which agree with the corresponding equations of specification GB 50017-2017 and AIJ, i.e.,  $N_{ut}/N_{uc}=0.78(2\gamma)^{0.2}$  and  $N_{ut}/N_{uc}=0.71\gamma^{0.3}$ . It can be seen from Fig. 9b that the

ratio  $N_{ut}/N_{uc}$  generally increases as  $\beta$  increases, and  $N_{ut}/N_{uc}$  increases slightly and obviously for  $\beta < 0.75$  and  $\beta > 0.75$  respectively. Furthermore, an exponential function is able to reasonably fit  $N_{ut}/N_{uc}-\beta$  curves when  $\beta \geq 0.8$ .

Based on the above FE parameters analysis results, the tensile-to-compressive capacity ratio  $N_{ut}/N_{uc}$  can be expressed as  $f_1(\gamma)f_2(\beta)$ . As for the CHS X-joints with  $\beta < 0.75$ , the predict equation of the ratio  $N_{ut}/N_{uc}$  can use the relevant equation of the specification of GB 50017-2017 or AIJ (i.e.,  $f_2(\beta)=1.0$  and  $f_1(\gamma)=0.78(2\gamma)^{0.2}$  or  $0.71\gamma^{0.3}$ ). For the X-joints with  $\beta > 0.75$ , the predict equation of  $N_{ut}/N_{uc}$  adopted a function of  $C_0\gamma^{C_1}\exp(C_2\beta)$ .  $C_0$ ,  $C_1$  and  $C_2$  are constant coefficients, which determined by regression analysis. Finally, the equation for the ratio  $N_{ut}/N_{uc}$  is established and expressed as following:

$$N_{ut}/N_{uc} = 0.02\gamma^{0.61} \exp(3.68\beta) \quad (4)$$

There are total 50 data (including FE data and test data) are utilized to evaluate predict equation of the ratio  $N_{ut}/N_{uc}$  of the two specifications (GB 50017-2017 and AIJ), as shown in Fig. 10. These 50 data are also used to evaluate the predict equation proposed in the paper, i.e., the equation of GB50017-2017 for  $\beta < 0.75$  and Eq. (4) for  $\beta \geq 0.8$ , as shown in Fig. 11. In the Figs. 10 and 11, abscissa is geometric parameters  $\beta$ , ordinate is relative errors (RE) between FE results and predicted results of these equations. It can be seen from Fig. 10 that most of RE are within 10% for



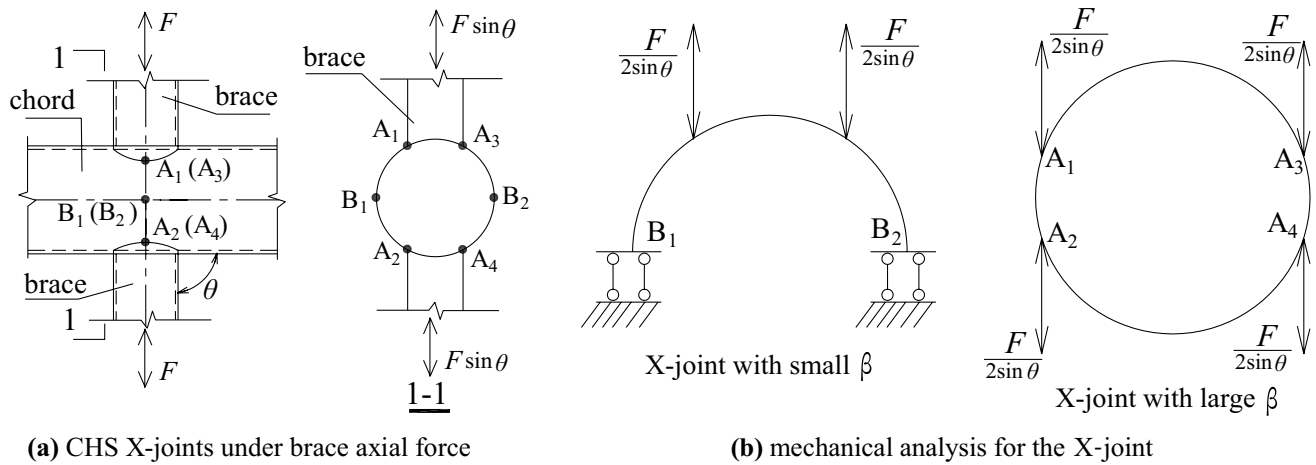
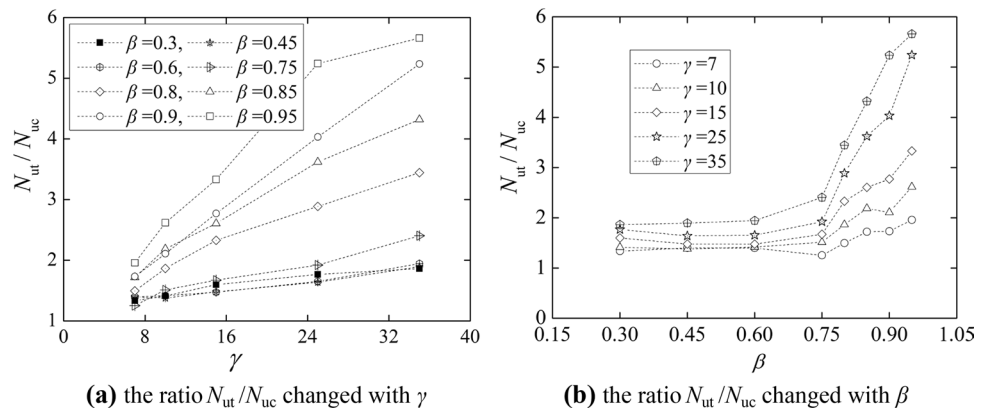


Fig. 8 Mechanical performance comparison between the X-joint with large  $\beta$  and with small  $\beta$

Fig. 9 Effect of the parameters  $\beta$  and  $\gamma$  on the tensile-to-compressive capacity ratio  $N_{ut}/N_{uc}$



$\beta \leq 0.75$ , but most of RE are larger than 25% for  $\beta \geq 0.8$ , which means the equations of the two specifications (GB 50017-2017 and AIJ) is difficult to accurately predict these  $N_{ut}/N_{uc}$  ratios with relative larger  $\beta$  ( $\geq 0.8$ ). Figure 11 shows that most of RE within 15% for  $\beta \geq 0.8$ , which implied Eq. (4) can well reflect these  $N_{ut}/N_{uc}$  ratios with relative larger  $\beta$  ( $\geq 0.8$ ). As for the  $\beta$  form 0.75 to 0.8, the predict value of  $N_{ut}/N_{uc}$  adopt linear interpolation between Eq. (4) and the equation of GB50017-2017.

### 5 Conclusions

Two experimental of CHS X-joints are performed to study the behavior difference under brace compression loaded and brace tension loaded. The test results are also utilized to calibrate FE model. Then, FE parameters analysis is perform to investigate the tensile-to-compressive ultimate capacity ratio  $N_{ut}/N_{uc}$ . Moreover, the relationship between  $N_{ut}$  and  $N_{uc}$  mentioned in the current specifications are also evaluated, and the corresponding improvement is

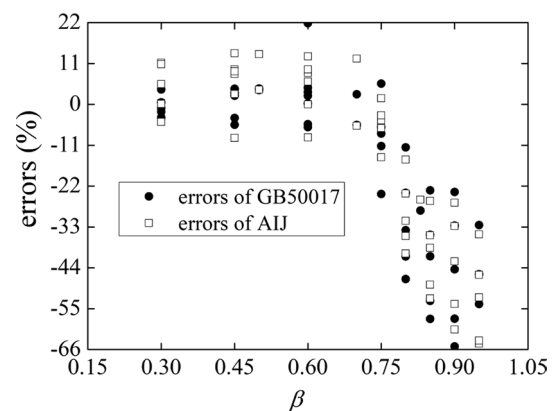
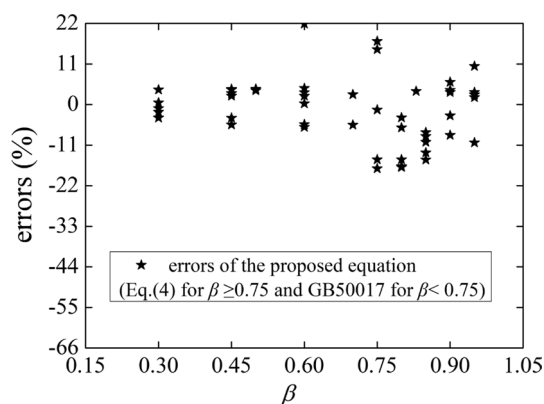


Fig. 10 Errors of  $N_{ut}/N_{uc}$  for GB 50017-2017 and AIJ

proposed. Finally, a new equation for the ratio  $N_{ut}/N_{uc}$  is established to accurately predict the difference between the tensile capacity and the compressive capacity of the X-joints with relative larger  $\beta$  ( $\geq 0.8$ ). The paper mainly draws the following conclusions:



**Fig. 11** Errors of  $N_{ut}/N_{uc}$  for the proposed predict equation

1. The finally failure mode of CHS-MC (the specimen under brace compression load) is buckling of chord wall near brace/chord intersection, and the failure mode of CHS-AR (the specimen under brace axial cyclic loaded) is the tearing of the chord wall near the brace/chord intersection. Both specimens showed good ductility, and their peak load is close to the resistance corresponding to the connection deformation of 3% of chord diameter (limit deformation criterion).
2. Both experimental results and FE results show that the tensile capacity ( $N_{ut}$ ) is significantly greater than the corresponding compressive capacity ( $N_{uc}$ ). Moreover, the ratio  $N_{ut}/N_{uc}$  increases not only with the increase of the parameter  $\gamma$  (chord radius-to-thickness ratio) but also with the increase of the parameter  $\beta$  (the ratio of brace diameter to chord diameter), especially when  $\beta > 0.75$ .
3. An equation for the ratio  $N_{ut}/N_{uc}$ , considering the effects of both  $\gamma$  and  $\beta$ , is proposed and has been validated favorably.

**Acknowledgements** The financial support from the Zhejiang Provincial Natural Science Foundation (No. LY20E080020); the China Scholarship Council (Nos. 201708330384, 201707005100), the National Natural Science Foundation of China (No. 51778538) and the China-Indonesia Joint Research Center for High-speed Railway Technology (No. KY201801005) are acknowledged and sincerely appreciated by the authors.

## References

- Abaqus Documentation. (2016). *Abaqus analysis user's manual* [OL]. AIJ. (1997). *Recommendations for the design and fabrication of tubular truss structures in steel*. Tokyo: Architectural Institute of Japan. (in Japanese).
- BS EN 1993-1-5:2006. (2006). Eurocode 3. Design of steel structures. Part 1–5: Plated structural elements. STANDARD by British-Adopted European Standard (pp. 45–48).
- Chen, Y., Feng, R., & Xiong, L. L. (2016). Experimental and numerical investigations on double-skin CHS tubular X-joints under axial compression. *Thin-Walled Structures*, 106, 268–283.
- Chinese Standard GB 50017–2017. (2018). *Standard for design of steel structures*. Beijing: Chinese Standard GB 50017–2017. (in Chinese).
- Choo, Y. S., Qian, X. D., Liew, J. Y. R., et al. (2003). Static strength of thick-walled CHS X-joints—Part I. New approach in strength definition. *Journal of Constructional Steel Research*, 59, 1201–1228.
- EN 1993-1-8:2005, Eurocode 3. (2005). *Design of steel structures Part 1–8: Design of joints*. Brussels: European Committee for Standardization.
- Feng, R., & Young, B. (2015). Theoretical analysis of cold-formed stainless steel tubular joints. *Engineering Structures*, 83, 99–115.
- Forti Nádia, C. S., Requena João Alberto, V., & Forti Tiago, L. D. (2015). Parametric study of tubular KK multiplanar steel connections. *Journal of Constructional Steel Research*, 114, 188–195.
- Gerdeen, J. C. (1980). *A critical evaluation of plastic behavior data and a united definition of plastic loads for pressure components*. New York: Welding Research Council Bulletin.
- Hassanipour, A., Rahnavard, R., & Mokhtari, A. (2016). Numerical investigation on reduces web beam section moment connections under the effects on cyclic loading. *Journal of Mechanical Engineering Science and Technology*, 2(8), 3159-0040.
- Hosseini, S. M., & Rahnavard, R. (2020). Numerical study of steel rigid collar connection affecting cyclic loading. *Engineering Structures*, 208(2020), 110314.
- Iskander, M. S., Shaat, A. A., Sayed-Ahmed, E. Y., et al. (2017). Strengthening CHS T-joints subjected to brace axial compression using through-bolts. *Journal of Constructional Steel Research*, 128, 555–566.
- Kurobane, Y., Makino, Y., Ochi, K., et al. (1984). Ultimate resistance of unstiffened tubular joints. *Journal of Structural Engineering, ASCE*, 110(2), 385–400.
- Lan, X. Y., Wang, F., Ning, C., et al. (2016). Strength of internally ring-stiffened tubular DT-joints subjected to brace axial loading. *Journal of Constructional Steel Research*, 125, 88–94.
- Lesani, M., Bahaari, M. R., & Shokrieh, M. M. (2014). Experimental investigation of FRP-strengthened tubular T-joints under axial compressive loads. *Construction Build Materials*, 53, 243–252.
- Lesani, M., Bahaari, M. R., & Shokrieh, M. M. (2015). FRP wrapping for the rehabilitation of Circular Hollow Section (CHS) tubular steel connections. *Thin-Walled Structures*, 90, 216–234.
- Liu, C., & Fang, D. (2020). Robustness analysis of vertical resistance to progressive collapse of diagrid structures in tall buildings. *The Structural Design of Tall and Special Buildings*. <https://doi.org/10.1002/tal.1775>.
- Liu, C., Li, Q., Zheng, L., et al. (2018). A review of the diagrid structural system for tall buildings. *The Structural Design of Tall and Special Buildings*. <https://doi.org/10.1002/tal.1445>.
- Liu, C., Luo, X., Fang, D., et al. (2019). Study on flexural stiffness of diagrid non-stiffened node based on four-spring assemblage model. *Engineering Structures*. <https://doi.org/10.1016/j.engstruct.2019.109500>.
- Liu, C. Q., & Ma, K. Q. (2017). Calculation model of the lateral stiffness of high-rise diagrid tube structures based on the modular method. *The Structural Design of Tall and Special Buildings*. <https://doi.org/10.1002/tal.1333>.
- Liu, C. Q., Ma, K. Q., Wei, X. D., et al. (2017). Shaking table test and time-history analysis of high-rise diagrid tube structure. *Periodica Polytechnica-Civil Engineering*, 61(2), 300–312. <https://doi.org/10.3311/PPci.9243>.
- Liu, C., Zhao, B., Yang, J., et al. (2020). Effects of brace-to-chord angle on capacity of multi-planar CHS X-joints under out-of-plane bending moments. *Engineering Structures*. <https://doi.org/10.1016/j.engstruct.2020.110434>.

- Lu, L. H., Winkel, G. D., Yu, Y., et al. (1994). Deformation limit for the ultimate strength of hollow section joints. In *Sixth international symposium on tubular structures, Melbourne*.
- Naghavi, M., Rahnavard, R., Thomas, R., et al. (2019). Numerical evaluation of the hysteretic behavior of concentrically braced frames and buckling restrained brace frame systems. *Journal of Building Engineering*, 22, 415–428.
- Nassiraei, H., Lotfollahi-Yaghin, M. A., & Ahmadi, H. (2016). Static performance of doubler plate reinforced tubular T/Y subjected to brace tension. *Thin-Walled Structures*, 108, 138–152.
- Rahnavard, R., Hassanipour, A., & Mounesi, A. (2016). Numerical study on important parameters of composite steel-concrete shear walls. *Journal of Constructional Steel Research*, 121, 441–456.
- Rahnavard, R., Hassanipour, A., & Siahpolo, N. (2015). Analytical study on new types of reduced beam section moment connections affecting cyclic behavior. *Case Studies in Structural Engineering*, 3, 33–51.
- Rahnavard, R., Naghavi, M., Aboudi, M., et al. (2018). Investigating modeling approaches of buckling-restrained braces under cyclic loads. *Case Studies in Construction Materials*, 8, 476–488.
- Togo, T. (1967). *Experimental study on mechanical behavior of tubular joints*. Osaka: Osaka University.
- Voth, A. P., & Packer, J. A. (2012). Numerical study and design of skewed X-type branch plate-to-circular hollow section connections. *Journal of Constructional Steel Research*, 68, 1–10.
- Xie, K. Z., Wang, H. W., Pang, J. H., et al. (2019). Study of the ultimate bearing capacity of concrete-filled steel tube K-joints. *KSCE Journal of Civil Engineering*, 23(5), 2254–2262.
- Zhao, B. D., Fang, C., Wang, W., et al. (2019a). Seismic performance of CHS X-connections under out-of-plane bending. *Journal of Constructional Steel Research*, 158, 591–603. <https://doi.org/10.1016/j.jcsr.2019.04.019>.
- Zhao, B. D., Ke, K., Liu, C. Q., et al. (2020). Computational model for the flexural capacity and stiffness of eccentric RHS X-connections under brace out-of-plane bending moment. *Journal of Structural Engineering*. [https://doi.org/10.1061/\(ASCE\)ST.1943-541X.0002507](https://doi.org/10.1061/(ASCE)ST.1943-541X.0002507).
- Zhao, B. D., Liu, C. Q., Yan, Z. X., et al. (2019b). Semi-rigidity connection model for unstiffened CHS X-type joints subjected out-of-plane bending. *International Journal of Steel Structures*, 19(3), 834–849. <https://doi.org/10.1007/s13296-018-0168-x>.

**Publisher's Note** Springer Nature remains neutral with regard to jurisdictional claims in published maps and institutional affiliations.